

Review

Quantum Light Source Based on Semiconductor Quantum Dots: A Review

Rusong Li ^{1,2,3}, Fengqi Liu ^{1,4} and Quanyong Lu ^{1,*}

¹ Division of Quantum Materials and Devices, Beijing Academy of Quantum Information Sciences, Beijing 100193, China; lirs2022@baqis.ac.cn (R.L.); fqliu@semi.ac.cn (F.L.)

² Beijing National Laboratory for Condensed Matter Physics, Institute of Physics, Chinese Academy of Sciences, Beijing 100190, China

³ School of Physical Sciences, University of Chinese Academy of Sciences, Beijing 100049, China

⁴ Key Laboratory of Semiconductor Materials Science, Institute of Semiconductors, Chinese Academy of Sciences, Beijing 100083, China

* Correspondence: luqy@baqis.ac.cn

Abstract: Quantum light sources that generate single photons and entangled photons have important applications in the fields of secure quantum communication and linear optical quantum computing. Self-assembled semiconductor quantum dots, also known as “artificial atoms”, have discrete energy-level structures due to electronic confinement in all three spatial dimensions. It has the advantages of high stability, high brightness, deterministic, and tunable emission wavelength, and is easy to integrate into an optical microcavity with a high-quality factor, which can realize a high-performance quantum light source. In this paper, we first introduce the generation principles, properties, and applications of single-photon sources in the field of quantum information and then present implementations and development of quantum light sources in self-assembled semiconductor quantum dot materials. Finally, we conclude with an outlook on the future development of semiconductor quantum dot quantum light sources.

Keywords: quantum information; single-photon source; entangled photon source; semiconductor quantum dots



Citation: Li, R.; Liu, F.; Lu, Q. Quantum Light Source Based on Semiconductor Quantum Dots: A Review. *Photonics* **2023**, *10*, 639. <https://doi.org/10.3390/photonics10060639>

Received: 6 April 2023

Revised: 28 April 2023

Accepted: 20 May 2023

Published: 1 June 2023



Copyright: © 2023 by the authors. Licensee MDPI, Basel, Switzerland. This article is an open access article distributed under the terms and conditions of the Creative Commons Attribution (CC BY) license (<https://creativecommons.org/licenses/by/4.0/>).

1. Introduction

With the rapid development of an information-based society, the demand for high-speed information processing and secure information communication is undergoing a tremendous increase. At present, integrated circuit technology is approaching the physical limits in terms of material and process technologies. Moore’s law [1] is slowing down gradually, and the development of traditional computing technology is facing a systemic dilemma. Quantum information technology, based on the principles of quantum mechanics, provides a solution to future needs to a certain extent. Since quantum information was proposed in 1982 [2], with the establishment of quantum key distribution [3], Deutsch–Jozsa equilibrium function algorithm [4], invisible quantum transfer [5], Shor large number prime factorization algorithm [6], Grover’s search algorithm [7], etc., quantum communication [8], quantum computing [9], quantum storage [10], and quantum radar [11], has gained an exceptionally rapid development. In particular, the three quantum technologies with quantum light sources, quantum coding, regulation and transmission, and single-photon emission and detection as the core are the key parts of developing quantum communication. Studies have shown that quantum communication based on single-photon sources has an absolute security and high efficiency, whereas the acquisition of reliable and easily available single-photon sources is a bottleneck to promoting the development of related technologies. Therefore, an in-depth study of high-quality single-photon sources becomes of great value. Quantum bits, as the most fundamental unit of quantum information, can be physically

realized in a variety of systems, including photons, cold atoms, ion traps, superconducting loops, nuclear spins, etc. [12–16]. Among them, optical quantum bits as flying quantum bits are an excellent choice for quantum communication and quantum computing. Currently, the main methods for preparing single-photon states are attenuating laser sources [17], i.e., using spontaneous nonlinear optical processes in nonlinear materials [18] and spontaneous radiation generation of single photons from two-energy systems based on different atoms or atom-like levels, such as single atoms [19], single molecules [20], diamond color centers [21], defect states in two-dimensional materials [22,23], and semiconductor quantum dots (QDs) [24]. Among them, the semiconductor QDs are a kind of quasi-zero-dimensional nanometer material and have excellent photonic properties, which can be used to generate single photons and entangled photon pairs. Furthermore, the linewidth of their emitted photons is the ability to be radiative lifetime limited, and it is highly compatible with modern semiconductor manufacturing processes, enabling large-scale integration and scaling of quantum emitters on semiconductor chips. Therefore, semiconductor QD technology is one of the best solutions for single-photon sources to move further toward practicality.

In this work, we take a single photon as the carrier of quantum information. We first introduce the performances and principles of single-photon sources. Then, we introduce the realization and development of single-photon sources and entangled photon sources based on semiconductor QDs, especially for semiconductor QD single-photon sources and entangled photon sources with artificial microstructure enhanced emission. Finally, we summarize prospects for the future development of quantum light sources based on semiconductor quantum dots.

2. Ideal Single Photon Source

From the statistical point of view of light emission, light has been divided into two main categories: classical light sources containing thermally radiated light with coherent light and non-classical light sources containing fluorescently radiated light [25]. The photons emitted from a typical ordinary thermal radiation light source represented by incandescent lamps exhibit Bunching, which satisfies the Super Poissonian in terms of photon number distribution and is characterized by a very high probability of simultaneous reception of multiple photons within a short delay time interval. The coherent light source represented by the laser, which emits photons with randomization, satisfies the Poissonian distribution, which shows that the probability of detecting two photons at the same time is the same. There is neither a fixed time interval nor any correlation between the two photons. In contrast, the quantum light source is represented by the single-photon source, which emits photons showing antibunching, which satisfies the Sub Poissonian distribution and exhibits no simultaneous detection of two photons at the zero moment ($t = 0$) and a fixed time interval between the successive emitted photons.

The ideal single-photon source has and produces only one photon at a time. The main criteria for judging the quality of a single-photon source are two-photon suppression, indistinguishability, and efficiency.

2.1. Single-Photon Purity

It is essential to develop precise experimental methods to assess the quality of a single-photon source. Is a very important index for judging a single-photon source is the second-order correlation function $g^{(2)}(\tau)$; the photon statistics of a quantum state of light are determined by recording $g^{(2)}(\tau)$ defined as [26]:

$$g^{(2)}(\tau) = \frac{\langle \hat{a}^\dagger(t) \hat{a}^\dagger(t + \tau) \hat{a}(t + \tau) \hat{a}(t) \rangle}{(\langle \hat{a}^\dagger(t) \hat{a}(t) \rangle)^2} \quad (1)$$

where \hat{a} and \hat{a}^\dagger are annihilation and creation operators for the optical mode probed in the experiment. $g^{(2)}(\tau)$ indicates the probability of detecting a photon at each moment t and $t + \tau$. The $g^{(2)}(0) = 1 - 1/N$ for the Fock state with photon number N . Only the superposition

of the single-photon state and the vacuum state can get $g^{(2)}(0) = 0$. All other states obtain this value as positive, so the closer this value is to 0, the better the single-photon nature is. At that time, $g^{(2)}(0) = 0$, the probability of multiphoton is 0, and the anti-collective beam effect is presented. In addition, $g^{(2)}(0) = 1$ for ordinary coherent light (laser) and $g^{(2)}(0) = 2$ for thermal sources, $g^{(2)}(0)$ can be employed as a measure of the single-photon purity of a light source. Experimentally, the second-order correlation function of photons is generally measured by the Hanbury Brown and Twiss (HBT) interferometer [27] shown in Figure 1.

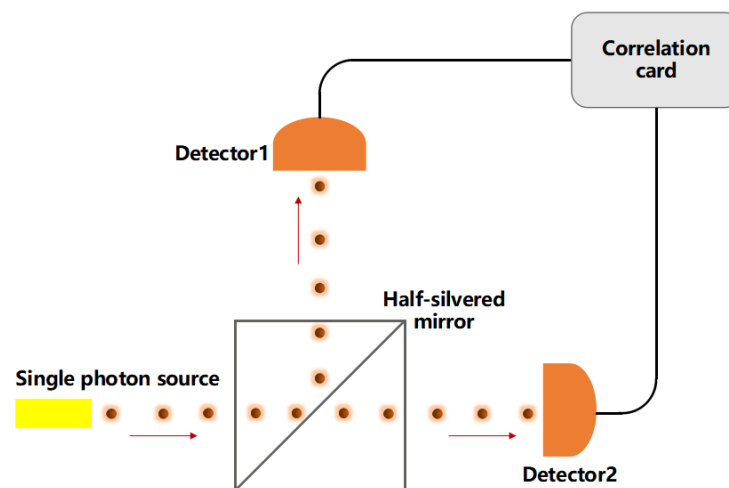


Figure 1. HBT interferometer to detect the second-order correlation coefficient $g^{(2)}(0)$.

2.2. Photon Indistinguishability

The single-photon source with only two-photon suppression cannot fully meet the application requirements of linear optical quantum computing and quantum networks. Since photon identity plays an important role in the realization of double-bit or multi-bit quantum logic gates, single-photon sources are also required. The photons emitted by the source are identical. When a photon is incident on a 50:50 beam splitter, it will be transmitted or reflected with half the probability. When two identical photons are incident from both ends of the beam splitter, the following four possible results will appear. Since the photon will introduce a phase jump of $\pi/2$ when reflected on the beam splitter, the corresponding probability amplitude distributions of the four situations are shown in Figure 2. The two cases in the middle of Figure 2 cancel out because the probability amplitudes are opposite, and the two photons are emitted in the same direction. This phenomenon is Hong–Ou–Mandel (HOM) interference [28]. In experiments, the photon indistinguishability is judged by measuring the HOM interference contrast of two photons emitted by a single quantum dot. The luminescent dipoles in the atomic-like structure are often in a complex lattice environment, affected by lattice vibrations (phonons), resulting in decoherence and broadening of the energy spectrum of the fluorescent photons, thereby reducing photon indistinguishability.

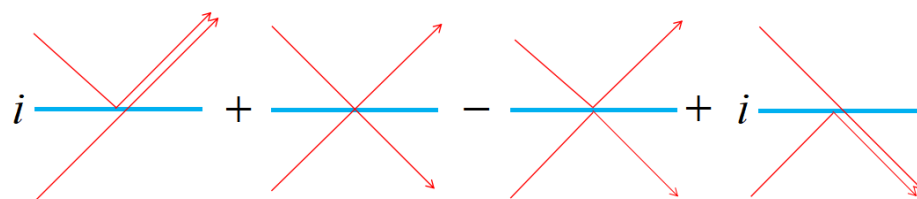


Figure 2. The possible output results and probability amplitudes of two photons incident through a 50:50 beam splitter.

2.3. Single-Photon Efficiency

The efficiency includes the single-photon generation efficiency and the collection efficiency. The single-photon generation efficiency is the probability that a single photon is produced by a single-photon source under a single pulse excitation. For an ideal deterministic single-photon source, one and only one photon is produced for each pulse excitation. Since the QD is inside a high refractive index group III-V semiconductor material, when photons exit the sample, most of the photons cannot be collected effectively by the optical system due to total reflection. As shown in Figure 3a, for example, for the interface between GaAs ($n_1 = 3.59$) and air ($n_2 = 1$), the angle of total reflection inward is small:

$$\theta_c = \arcsin \frac{n_2}{n_1} = 16.17^\circ \quad (2)$$

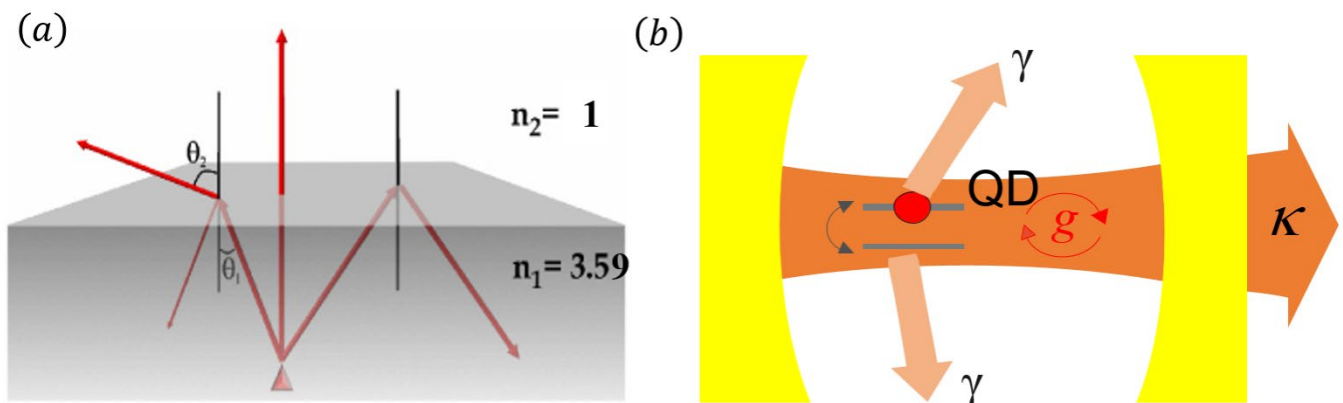


Figure 3. (a) Schematic diagram of the inward total reflection angle of GaAs material; (b) Interaction of the two-energy system with the cavity.

When the angle of incidence of photons arriving at the GaAs surface is greater than θ_c , the photons will be completely reflected inward and cannot be detected by the detector. Where the outgoing stereo angle of photons leaving the GaAs surface is:

$$\Omega = 2\pi(1 - \cos \theta_c) = 2\pi \left[1 - \sqrt{1 - \left(\frac{n_2}{n_1} \right)^2} \right] \approx 0.249 \quad (3)$$

Since photons generated by a single-photon source tend to exit along a 4π space angle, the collection efficiency is:

$$\eta = \Omega/4\pi \approx 2\% \quad (4)$$

Clearly, the low collection efficiency is due to the lack of a proper cavity for strong coupling and efficient outcoupling.

The generation of single photon or photon pairs in QD is deterministic in its nature. However, efficient extraction of single photon or photon pairs from the high index semiconductor material requires the engineering of the photonic environment. In fact, the extraction efficiency can be even lower, considering the factors such as sample surface roughness and material absorption. Therefore, there is a great need to enhance the photon collection efficiency. Experimentally, researchers usually use the method of optical microcavities or waveguide structures (such as nanowires, microlenses, metasurfaces, etc.) to enhance the efficiency of photon extraction. Figure 3b shows the typical single-photon source consisting of a single QD coupled coherently, with coupling constant g , to one mode of a Fabry–Pérot cavity. Incoherent processes are spontaneous emission from the nonclassical light emitter to the continuum at rate γ and photon loss through the cavity mirrors at rate κ . Integrating quantum dots into optical microcavities can channel the spontaneously emitted photons into a well-defined spatial mode and in a desired direction to improve the overall efficiency.

It can alter the spectral width of the emission. It can also provide an environment where dissipative mechanisms are overcome so that a pure quantum-state emission takes place. By coupling with an optical microcavity, the interaction between the cavity mode and quantum energy levels can be greatly enhanced. Depending on the relationship between the strength of the coupling and the decay rate, the coupling system can be divided into weakly coupled and strongly coupled systems [29,30]. In the strong coupling region [31], the intrinsic energy of semiconductor quantum dot energy level and microcavity optical field mode coupling is split, and the split energy is [32]:

$$E_{1,2} = \frac{E_c + E_x}{2} - \frac{i(\gamma_c - \gamma_x)^2}{4} \pm \sqrt{g^2 - \frac{(\gamma_c - \gamma_x)^2}{16}} \quad (5)$$

where E_x and E_c are the energies of the QD exciton and cavity modes, γ_x and γ_c are their full-width half-maximum (FWHM), $\Delta = E_x - E_c$ is the detuning, and g is the exciton-cavity coupling strength. Strong coupling requires $g^2 > (\gamma_c - \gamma_x)^2/16$, which leads to a splitting of the two eigenenergies at resonance ($\Delta = 0$) by an amount called the vacuum Rabi splitting. For typical QD and microcavities, γ_x (a few μeV) is much smaller than γ_c ($\sim 100 \mu\text{eV}$), and the strong coupling condition reduces to $g > \gamma_c/4$. In order to reach strong coupling with a given oscillator strength, one must maximize the ratio of cavity quality factor to mode volume [33]. In addition, in the strong-coupling regime, due to the coupling of the QD to a privileged cavity mode is far stronger than its coupling to all other modes, so the ensuing process of spontaneous emission becomes deterministic.

When the coupling strength is less than the decay rate, the coupling system is weakly coupled. In this case, the spontaneous radiation rate of the QD is enhanced due to the increase of the local field density of states, and the enhancement is a multiple of the Purcell factor, which is the Purcell effect. It, therefore, can be used to optimize the performance of optical devices such as lasers and quantum light sources. The maximum Purcell factor is obtained when the QD is located at the position with the maximum field strength [34,35]:

$$F_p = \frac{3}{4\pi^2} \left(\frac{\lambda}{n} \right)^3 \frac{Q}{V} \quad (6)$$

where λ is the resonant wavelength, n is the refractive index of the dielectric material in the microcavity, Q is the quality factor of the cavity, and V is the mode volume in the cavity. In fact, F_p will be far from the optimal value because of the existence of detuning between quantum dots and microcavities and other problems. When $F_p < 1$, the spontaneous radiation rate of quantum dots will be suppressed; when $F_p > 1$, the spontaneous radiation rate of quantum dots will be enhanced, which means more single photons will be radiated by quantum dots per unit time. From the definition, it can be seen that a small mode volume and a large quality factor can lead to an increase in the spontaneous radiation rate. The microcavity structure that can be coupled with the QD can effectively modulate the quantum dot luminescence performance by a proper design of microcavity parameters and the combination of semiconductor growth process conditions of the microcavity structure. When the QDs are located in the center of the cavity mode, the QD and the cavity can achieve good coupling efficiency ($\beta = \frac{F_p}{1+F_p}$), and it will play a great role in enhancing the emission rate of QD.

3. Self-Assembled Semiconductor Quantum Dots

3.1. Growth of Self-Assembled Semiconductor Quantum Dots

Currently, single-photon emission has been experimentally observed in different atomic and atom-like systems such as atoms, ions, molecules, NV color centers, and QD. Among them, the growth of self-assembled semiconductor QD mainly by molecular beam epitaxy (MBE) or metal-organic compound chemical vapor deposition (MOCVD) is of great interest because of its solid-structure stability and discrete atom-like energy level structure

recognized as a strong contender for achieving high-quality single-photon sources in solid-state systems. In addition, QDs can be excited with double excitons or even multiple excitons, generating frequency-distinguishable photon pairs or a sequence of photons of different frequencies through a cascade of fouling processes, each of which is a single photon at each frequency.

InAs/GaAs QDs are a kind of self-assembled semiconductor nanostructures that are widely studied in experiments nowadays. It is generally formed by growing InAs QD on GaAs material in Stranski–Krastanow (S–K) growth mode [36]. Since there is a constant lattice mismatch of about 7% on GaAs, InAs adapt to the lattice mismatch by elastic strain. Figure 4a is a schematic diagram of the constant lattice variation in growing dislocation-free InAs QD on GaAs substrate through the S–K growth mode. The GaAs buffer layer is grown first, and then the precipitation of InAs continues on the GaAs buffer layer. Initially, InAs is grown in two dimensions to form the infiltrated layer. Since the InAs lattice structure is larger than that of the GaAs substrate, the epitaxial layer is compressed laterally, and stress is generated, which increases with the thickness of InAs. When the deposited amount exceeds the critical value, the accumulated elastic energy is released, and the three-dimensional growth begins, forming InAs QDs. The QDs are formed randomly on the surface of GaAs material, and the height of these QDs is around 1~10 nm, and the diameter is around 10~70 nm, as shown in Figure 4b [37]. The size of the dots has a great influence on the spectral lines of QD fluorescence, and the larger the difference in the size of QDs, the larger the difference in the fluorescence emission wavelength of QDs. In addition, due to the random distribution of self-assembled semiconductor QD leading to a very low yield of single-photon sources, in order to make the QD coupled to microcavities controllable, the determination of the position of the self-organized grown QD using different optical positioning methods (without damage) has been proposed [38,39]. It should be noted that the semiconductor QD growth method given here is not limited to InAs/GaAs QDs, but is also applicable to QDs of other semiconductor materials.

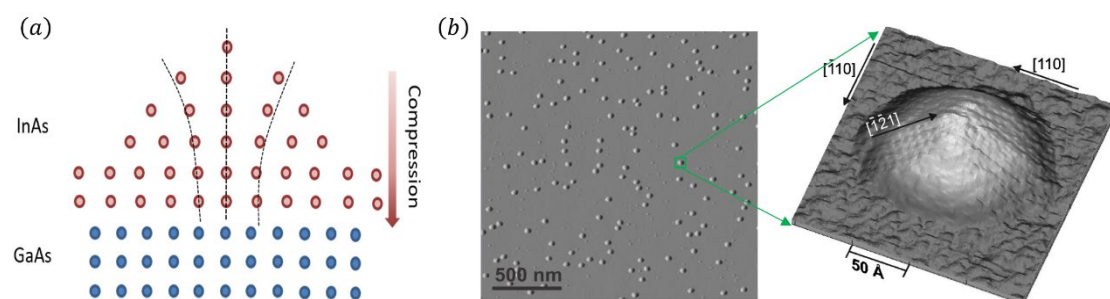


Figure 4. (a) Lattice mismatch on InAs/GaAs material; (b) AFM images of self-organized grown InAs/GaAs QD, the bright spot-like structures are typical of QD with lateral diameters of 10~70 nm and heights of 1~10 nm. Inset: shows a three-dimensional scanning tunneling microscopy image of an uncovered InAs QD grown on GaAs (001) [37]. (b) inset from Ref [37], reprint with the permission of AIP Publishing).

3.2. Band Structure of Self-Assembled Semiconductor Quantum Dots

Since the size of the MBE-grown self-assembled semiconductor QD in the growth direction is smaller than that in the lateral direction, the energy level splitting in the growth direction (z-direction) of the self-assembled semiconductor QD is much larger than the energy splitting in the lateral direction. For the InAs/GaAs QD shown in Figure 5a, the InAs QD material is grown in the GaAs material. The energy band of InAs/GaAs QD is divided into conduction bands and valence bands, in which the fluctuation equation of the ground state electron in the conduction band shows s-wave symmetry, the spin angular momentum of the electron is $1/2$, and the spin $S_z = \pm 1/2$ in the z-axis direction. In contrast, the ground state hole in the valence band shows p-wave symmetry. The angular momentum of the holes is $3/2$. The holes in the z-axis direction are divided into heavy

holes and light holes, with the spin component $J_z = \pm 3/2$ in the z-axis direction for heavy holes and $J_z = \pm 1/2$ in the z-axis direction for light holes; there is also a spin-orbit splitting energy band in the valence band, which has a spin of $S_z = 1/2$ and a spin of $J_z = \pm 1/2$ in the z-axis direction. Since the heavy hole levels are far apart, we consider only the effect of heavy holes when discussing the structure of the excitonic state of InAs/GaAs quantum dots. Optical excitation of semiconductor QD allows studying the energy level structure of QD, which also is the most common method to obtain single photons. Optically excited semiconductor QD can be divided into non-resonantly excited QDs (including band excitation and p-shell excitation) and resonantly excited QD (including pulsed resonant excitation-Raby oscillation and continuous resonant excitation-Mollow triplet state). Before the QD is excited, there are no additional charged particles inside the QD, and the excitation produces an electron-hole pair called neutral exciton $|X\rangle$ (Excitons are formed due to the Coulomb interaction of electrons and holes with each other), in which the electrons and holes occupy the lowest energy levels of the conduction band and valence band, respectively. Since the optical selection law dictates that only transitions with total angular momentum $M = \pm 1$ occur in photon absorption, if the spins of electrons and heavy holes are antiparallel, excitons with the angular momentum of ± 1 on the z-axis ($(S_z = 1/2, J_z = -3/2)$ or $(S_z = -1/2, J_z = 3/2)$) satisfy the transitions, it is called a bright exciton. If the spins of the electron and heavy hole are parallel and the angular momentum component of the exciton in the z-axis is ± 2 ($(S_z = 1/2, J_z = 3/2)$ or $(S_z = -1/2, J_z = -3/2)$) is forbidden transitions, it is called a dark exciton [40]. QDs with a high degree of structural symmetry emit fluorescence spectral lines without dark excitons, only bright excitons. However, when the symmetry is broken by external factors (e.g., transverse magnetic field), a mixture of bright and dark excitons is generated, and the dark exciton component also appears in the fluorescence spectral line emitted by the QD.

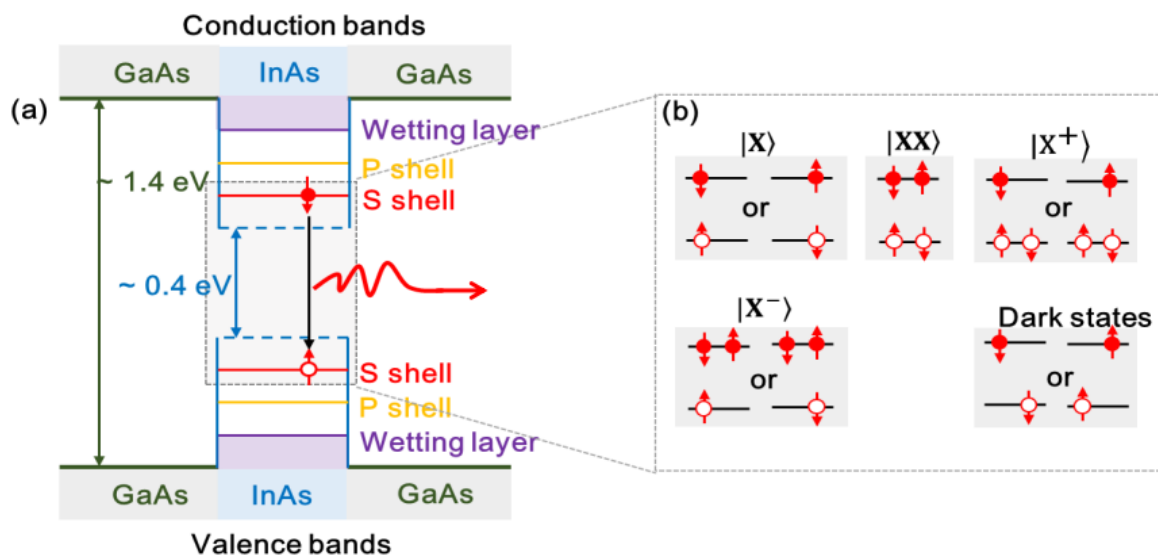


Figure 5. (a) Energy level structure of InAs/GaAs QD; (b) Schematic diagram of neutral exciton and charged exciton.

When the InAs/GaAs QD is excited through up the band, the photon energy of the excitation light is larger than the forbidden band width of GaAs around the QD. The electron-hole pair formed between the conduction band and the valence band undergoes a spontaneous relaxation process, and a part of the electrons and holes are trapped by the infiltration layer and then reach the lowest excited state of the QD after a phonon-assisted relaxation process of several tens of picoseconds to form an exciton. As shown in Figure 5b, when the QD captures an electron and a hole, a neutral exciton $|X\rangle$ is formed due to the Coulomb interaction between the electron and the hole. When the quantum dot captures two electrons and a hole, the exciton formed is the charged exciton $|X^- \rangle$. The same process

can occur with two holes and one electron $|X^+\rangle$, two electrons and two holes $|XX\rangle$ (double exciton), etc. In contrast to charged excitons, neutral excitons have exchange interactions between electrons and holes. Due to the irregularity of the QD growth process, there is fine structure cleavage of energy levels even without an external magnetic field, while in charged excitons, the total angular momentum of the two electrons in the conduction band is zero, and there are no exchange interactions. At the same time, the neutral exciton $|X\rangle$ has a Coulomb interaction of one electron and one hole, while the charged exciton $|X^-\rangle$ has a three-body Coulomb interaction of two electrons and one hole, and the energy of the charged exciton $|X^-\rangle$ is smaller than that of the neutral exciton. The Coulomb interactions of different excitons and the fluorescence photon energy emitted is also different. This Coulomb reformation process can be distinguished from the different exciton states of QD by spectral analysis, and the fluorescence generated by band excitation contains multiple exciton components. Since the excitation time from electron-hole generation to relaxation to exciton formation in QDs is less than the radiative lifetime of QD fluorescence (~ 1 ns), QDs have and will have only one fluorescent photon for each excitation. It should be noted that the analysis of the band structure of semiconductor QDs given here is not limited to InAs/GaAs QDs, but is also applicable to QDs of other semiconductor materials.

4. Artificial-Microstructure Enhanced Single Photon Emission from Single Semiconductor Quantum Dot

Next, we will review the development of research on several different types of artificial microstructures enhanced by single self-assembled semiconductor QD single-photon sources. Semiconductor cavities employing distributed Bragg reflectors (DBR), micropillars, and photonic crystals are used to enhance the repetition rate, collection efficiency, polarization, and indistinguishability of single photons. In 1999, Kim J. et al. achieved a similar flow of single photons emission with a well-regulated time interval in a GaAs/AlGaAs three-quantum well (QW) sandwich structure inside pillar microcavity for the first time at a temperature of 50 mK [41]; In 2000, Michler P et al. realized the single-photon source of InAs QDs coupled with the whispering gallery cavity mode in the microdisk cavity (which consists of a disk 5 μm in diameter and a 0.5 μm $\text{Al}_{0.65}\text{Ga}_{0.35}\text{As}$ post. The disk area consists of 100 nm of GaAs, an InAs QD layer, and 100 nm of GaAs.) [42]; In 2002, Yuan Z. et al. achieved electrically driven single-photon emission for the first time at a temperature of 5 K [43]; In the same year, Santori C et al. tested the indistinguishability of photons emitted from a semiconductor QD in a microcavity through a HOM-type two-photon interference experiment, they find that consecutive photons are largely indistinguishable, with a mean wave-packet overlap as large as 0.81 [44]. In 2005, Badolato A. et al. observed clear signatures of cavity QED (such as the Purcell effect) in all fabricated structures by achieving a deterministic spatial and spectral overlap between a QD exciton line and a photonic crystal cavities mode. This approach immediately found application in cavity-assisted QD spin-flip Raman transition to generate indistinguishable single photons [45]. In 2006, Chang W. H. et al. realized an efficient single-photon source based on low-density InGaAs QDs embedded in linear-type photonic crystal cavities, and the devices feature the effects of a photonic band gap, yielding a single-mode spontaneous emission coupling efficiency as high as 92%, a high degree of single-photon purity of $g^{(2)}(0) = 0.01$ and a linear polarization degree up to 95% [46].

Since then, the growth and fabrication processes of QD into different microcavities have been continuously improved to optimize the QD luminescence and microcavity optical field coupling performance, which has led to the rapid development of microcavities in enhancing the single-photon emission of semiconductor QD. Table 1 lists some of the reported single-photon sources based on III-V self-assembled semiconductor QDs between 2007 and 2015 in terms of luminescence wavelength, lifetime, second-order correlation function, and optical microcavity structures employed.

Table 1. Selected reports of single-photon sources based on semiconductor QDs [47–61].

Photonic Structure	Life Time (ns)	Wavelength (nm)	$g^2(0)$	References
Micropillar	0.65	~917	0.05	[47]
Micropillar	0.015	~956	0.18	[48]
Photonic crystal cavities	0.045	~944	0.05	[49]
Tapered nanowires	2.4	~915	<0.008	[50]
Photonic crystal cavities	~1	~1550	0.43 ± 0.04	[51]
Tapered nanowires	1.7 ± 0.1	~881	0.12	[52]
Photonic crystal cavities	0.2	~1550	0.10 ± 0.02	[53]
Photonic crystal cavities	0.87 ± 0.15	~910	0.27 ± 0.07	[54]
Nano-trumpet	0.82	~907	0.31	[55]
Micropillar	0.265–0.270	~932	0.05	[56]
Micropillar	~0.39	~941	0.012(2)	[57]
Photonic crystal cavities	1.61	~905	0.04 ± 0.05	[58]
Adiabatic pillar	0.14 ± 0.04	~945	0.10 ± 0.03	[59]
Microlens	~1	~925	<0.01	[60]
Circular Bragg grating(CBG) cavities	0.52	~907	0.009 ± 0.005	[61]

Single-photon sources based on semiconductor self-assembled QDs have attracted increasing attention due to their potential applications in quantum computing and quantum communication. In recent years, significant developments have been made in microcavity-enhanced semiconductor QD single-photon sources. In 2016, Ding X. et al. coupled QD to micropillar cavities (The QD was grown via molecular beam epitaxy, embedded in a λ -thick GaAs cavity, and sandwiched between 25.5 lower and 15 upper DBR stacks. Micropillars with 2.5 μm diameter were defined via electron beam lithography), as shown in Figure 6a. Under s-shell pulsed resonant excitation of a Purcell-enhanced QD micropillar, they deterministically generated resonance fluorescence single photons which, at π pulse excitation, had an extraction efficiency of 66%, single-photon purity of 99.1%, and photon indistinguishability of 98.5% [62]. In the same year, Somaschi N. et al. reported a single-photon source made of QD in electrically controlled micropillar cavities, as shown in Figure 6b [63]. The application of an electrical bias on the deterministically fabricated structures is shown to strongly reduce charge noise. Under resonant excitation, indistinguishability of 0.9956 ± 0.0045 is demonstrated with $g^{(2)}(0) = 0.0028 \pm 0.0012$. The photon extraction of 65% and measured brightness of 0.154 ± 0.015 make this source 20 times brighter than any source of equal quality. There are still huge challenges regarding electrically pumped single-photon sources based on semiconductor quantum dots, such as complicated fabrication processes, low collection efficiency, and how to effectively overcome the effects of charge noise, etc. In 2017, Heindel T. et al. introduced an attractive type of integrated twin-photon source based on a QD deterministically integrated within a monolithic microlens, as shown in Figure 6c. Triggered generation of photon pairs with the same energy and polarization becomes possible by utilizing a biexciton–exciton radiative cascade, where the biexciton binding energy equals the fine structure splitting of the bright exciton. They observed strong temporal correlations of the photon twins in auto-correlation measurements, resulting in a pronounced symmetric bunching peak. Further, by comparing the measured cross- and auto-correlation traces, they are able to determine the efficiency of the twin-photon cascade and demonstrate a HOM-type two-photon interference of (234 ± 4) kHz. In addition, they employ a photon-number-resolving detector to directly verify twin-photon emission and to reconstruct the photon number distribution emitted by the quantum emitter [64]. In 2018, Rongling Su et al. successfully demonstrated the up-converted excitation on single QDs for efficient generations of single photons using a pillar microcavity. By tuning the excitation laser frequency into the high-energy sidebands of the DBR in the micropillar while keeping the QD spectrally resonant with the cavity mode, they achieved bright on-demand single-photon emissions with a collection efficiency of $(77\% \pm 6\%)$ and a $g^{(2)}(0)$ of 0.044 ± 0.003 that is six times better than the value under above-band excitations [65]. However, it is difficult to fabricate both Bragg resonators with many

periodic thin layers using epitaxial methods and photonic crystals with periodic arrays of holes using electron beam lithography (EBL). In addition, surface plasmons in metallic structures have their intrinsic drawbacks, such as high optical losses, which can quench spontaneous emission, limiting their potential applications. The coupling of QDs to lossless all-dielectric photonic nanostructures based on high refractive index materials with optical response governed by multipolar Mie-type resonances has gained increasing popularity in recent years due to the simplicity in their fabrication is markedly easier. In 2017, Rutckaia V. et al. showed that Mie resonances govern the enhancement of the photoluminescent signal from embedded Ge(Si) QDs due to a good spatial overlap of the emitter position with the electric field of Mie modes. Based on the nanodisk mode engineering, they also show that the mode hybridization in a nanodisk trimer results in an up to 10-fold enhancement of the luminescent signal due to the excitation of resonant anti-symmetric magnetic and electric dipole modes [66]. In 2023, Kroychuk M K. et al. experimentally and numerically investigated the excitation of magnetic Mie-type resonance by linearly polarized light in a GaAs nanopillar oligomer with embedded InAs QD leads to quantum emitters absorption efficiency enhancement [67]. Moreover, they experimentally demonstrated more than ten times QDs photoluminescence (PL) enhancement and numerically reached forty times gain compared to unstructured film when the excitation wavelength is in the spectral vicinity of Mie-type resonance. We believe that QDs coupling with Mie-type resonant oligomers collective modes for nanoscale single-photon sources can be a promising candidate for next-generation quantum light sources for quantum information.

In 2020, Moczala-Dusanowska M. et al. demonstrated a Purcell-enhanced ($F_p = 3.5$) single-photon source realized by the fabrication of a hybrid III-V/dielectric circular Bragg grating (CBG) cavity directly bonded onto a piezoelectric actuator [68], as shown in Figure 6d. Such a kind of photonic system offers the potential for broadband high photon extraction efficiency and spontaneous emission rate enhancement. This device allows for reversible spectral tuning of the embedded quantum dot emitters and pure triggered single-photon generation with $g^{(2)}(0) = (1.5 \pm 0.05) \times 10^{-3}$, spontaneous emission lifetimes smaller than 200 ps. By applying 18 kV/cm electric field to the piezo substrate, they achieved a tuning range larger than 0.78 meV for QD in resonance with the cavity mode. In 2023, Li X. et al. presented a bright semiconductor single-photon source heterogeneously integrated with an on-chip electrically injected microlaser. The CBG is located right on top of the micropillar laser, and an additional spacer is designed specifically to separate cavity modes in each distinct component, as schematically shown in Figure 6e [69]. Different from previous one-by-one transfer printing techniques implemented in hybrid QD photonic devices, multiple deterministically coupled QD-CBG single-photon sources were integrated with electrically injected micropillar lasers at one time via a potentially scalable transfer printing process assisted by the wide-field photoluminescence (PL) imaging technique. Optically pumped by electrically injected microlasers, pure single photons are generated with a high brightness of count rate of 3.8 M/s and an extraction efficiency of 25.44%. Such a high brightness is due to the enhancement by the cavity mode of the CBG, which is confirmed by a Purcell factor of 2.5.

Single-photon sources in the telecommunication band have become a hot research topic in recent years due to their great advantage of extremely low loss in long-distance transmission in optical fibers. In the self-assembled quantum dot system, the InAs/InP system has been studied to produce single-photon sources in the O- and C-bands in the communication band. However, the refractive index difference between the two materials InP and InGaAsP, which form the distributed Bragg reflection cavity (DBR), is too small, which makes it difficult to form a DBR cavity with high-quality factor and affects the collection efficiency of single photons. In 2017, Chen Z. S. et al. obtained a high count rate single-photon emission at a wavelength of 1.3 μm with a photon extraction efficiency of 3.3% and the multi-photon emission possibility $g^{(2)}(0) = 0.14$ using InAs/GaAs bilayer QD coupled to a distributed Bragg reflector microcolumn cavity of 3 μm diameter. Cavity mode and Purcell enhancement have been observed clearly in microphotoluminescence

spectra [70]. In 2018, Liu F. et al. obtained a single-photon source with a high single-photon purity of 97.4% and indistinguishability of >90% in a waveguide-coupled QD–photonic crystal microcavity system by embedding a QD into a photonic crystal microcavity. Enhanced single-photon emission from semiconductor QD is observed due to the Purcell effect of the photonic crystal microcavity when using π -pulsed resonant excitation, as shown in Figure 6f. The radiation lifetime of the waveguide-coupled photonic crystal cavity system was shortened to 22.7 ps; this leads to near-lifetime-limited single-photon emission that retains high indistinguishability (93.9%) on a timescale in which 20 photons may be emitted [71].

In 2021, Kolatschek S. et al. achieved single-photon emission in the telecom O-band by coupling InGaAs/GaAs QD to a CBG cavity, yielding a Purcell enhancement by a factor of ~4, and bright single-photon emission is shown for transitions under above-band and p-shell pumping. When using p-shell pumping, a combination of high count rate with pure single-photon emission ($g^{(2)}(0) = 0.01$ in saturation) is achieved, and a good single-photon purity ($g^{(2)}(0) = 0.13$) together with a high detector count rate of 191 kcps is demonstrated for a temperature of up to 77 K [72]. In 2022, Xu S. W. et al. demonstrated bright telecom O-band single-photon sources based on In(Ga)As/GaAs QD deterministically coupled to hybrid CBG resonators using a wide-field fluorescence imaging technique [73]. It is worth mentioning that to ensure spatial overlaps between the QDs and hybrid CBG cavity, they used a wide-field fluorescence imaging technique to extract the positions of QDs respective to the pre-fabricated alignment marks. The QD emissions are redshifted toward the telecom O-band using an ultra-low InAs growth rate and an InGaAs strain-reducing layer. The single-photon source under both continuous wave (CW) and pulsed operations are demonstrated, showing high brightness with count rates of 1.14 MHz and 0.34 MHz under saturation powers and single-photon purities of $g^{(2)}(0) = 0.11 \pm 0.02$ (CW) and $g^{(2)}(0) = 0.087 \pm 0.003$ (pulsed) at low excitation powers. A Purcell factor of 4.2 with a collection efficiency of $11.2\% \pm 1\%$ at the first lens is extracted, suggesting an efficient coupling between the QD and hybrid CBG cavity.

By embedding QD into optical resonant cavities such as micro-pillar cavities and photonic crystal micro-cavities, the generated single photons that satisfy the Fourier transform limit relationship can be extracted with high efficiency. In recent years, despite the great improvement in the collection efficiency of quantum dots, the efficiency of polarized single-photon efficiency has hardly exceeded the 50% upper limit. There are two main reasons for this: the optical transition rules in quantum dots dictate that the polarization state of resonant fluorescence will be either random left-hand circular polarization or right-hand circular polarization. The other reason is that resonant excitation requires the suppression of pump light at the same frequency as the single photon, and the most efficient way to do this is to use an excitation-collection scheme with orthogonal polarization. This polarization filtering will simultaneously reduce the system efficiency of the quantum dot single photon by a factor of two. In 2019, Wang H. et al. proposed a high-performance semiconductor QD single-photon source based on narrowband elliptical micropillar cavities (which has a major (minor) axis of 2.1 μm (1.4 μm) and broadband elliptical CBG cavities (which consists of a central elliptical disk, surrounding elliptical grating and fully etched trenches. The major (minor) axis of the central elliptical disk is 770 nm (755 nm), the major (minor) axis period of the elliptical grating is 380 nm (372 nm), and the etching depth is 100 nm.), schemes for the experimental realization of a high-quality polarized single-photon source, as shown in Figure 7a,d [74]. The two non-degenerate fundamental modes of the elliptical micropillar cavity at 896.54 nm (labeled as M_1) and 897.04 nm (labeled as M_2), with a splitting of 183 GHz, as shown in Figure 7b. Figure 7c shows the polarization of M_1 (M_2) is parallel to the minor (major) axis, with a high degree of polarization of 99.7% (99.6%), which confirms the symmetry-broken, highly polarized nature of the elliptical micropillar cavity. The mode of the elliptical CBG cavities splits into a doublet (labeled as B1 and B2), and the splitting is 2.8 THz, which is 1.5 (1.3) times larger than the linewidth of B1 (B2), as shown in Figure 7e. Figure 7f shows with time-resolved resonance fluorescence measurements, the radiative

lifetime for the QD coupled to the elliptical micropillar cavity and the elliptical CBG cavity are $\sim 61.0(1)\text{ps}$ and $\sim 69.1(1)\text{ps}$, respectively, ~ 17.8 and ~ 15.7 times shorter than the average lifetime ($\sim 1.09\text{ }\mu\text{s}$) of more than 20 QDs in the slab from the same area. They demonstrated a polarized single-photon efficiency of 0.60 ± 0.02 (0.56 ± 0.02), a single-photon purity of 0.975 ± 0.005 (0.991 ± 0.003), and indistinguishability of 0.975 ± 0.006 (0.951 ± 0.005) for the elliptical micropillar (elliptical CBG) cavity. This work provides promising solutions for truly optimal single-photon sources combining near-unity indistinguishability and near-unity system efficiency simultaneously.

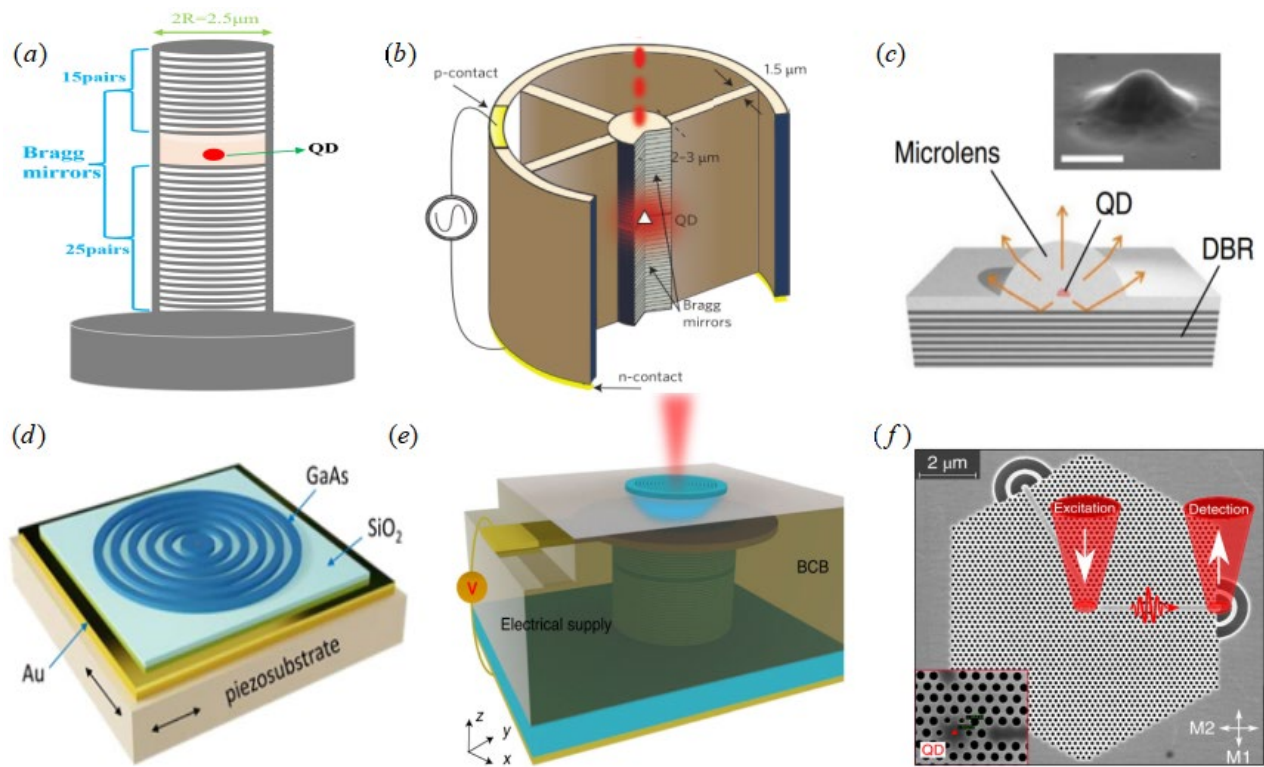


Figure 6. (a) An illustration of a single QD embedded in a micropillar; (b) Schematic of the electrically controlled single-photon sources: a micropillar coupled to a QD is connected to a surrounding circular frame by four one-dimensional wires [63]; ((b) from Ref [63], reprint with the permission of Springer Nature Publishing). (c) Illustration of our solid-state-based quantum light source constituted of a single QD deterministically integrated within a monolithic microlens [64]; ((c) from Ref [64], licensed under a Creative Commons Attribution 4.0 International License (CC BY 4.0)). (d) An artistic sketch of CBG cavity strain-tunable single-photon source composed of a 125 nm GaAs membrane with In (Ga)As QDs, a 360 nm layer of SiO₂, and a back reflecting gold mirror bonded to the piezo substrate [68]; ((d) from Ref [68], reprint with the permission of ACS Publishing). (e) Illustration of the bright semiconductor single-photon sources pumped by heterogeneously integrated micropillar lasers with electrical injections [69]; ((e) from Ref [69], licensed under a Creative Commons Attribution 4.0 International License (CC BY 4.0)). (f) Waveguide-coupled QD-H1 photonic crystal cavities single-photon sources [71]. ((f) from Ref [71], reprint with the permission of Springer Nature Publishing).

Photon spin states and orbital angular momentum (OAM) of photons are very important quantum resources [75,76], and on-demand tuned QD spin state single-photon sources and single-photon sources with orbital angular momentum are key devices for high-dimensional quantum information processing and have very important applications in fields such as quantum information and quantum chips. However, the random nature of single-photon radiation from QD leads to very difficult regulation of the spin state, and the integration of quantum devices cannot be achieved using traditional block optics such as beam splitters and wave sheets for regulation. Additionally, the generation of single

photons carrying orbital angular momentum is mostly probabilistic by nonlinear processes with low efficiency, which becomes a major bottleneck limiting the processing of high-dimensional quantum information. In 2020, Bao Y. et al. proposed a silicon-based metalens with a double focus to modulate the direction and spin state of the single-photon source radiation, as shown in Figure 8a [77]. In this structure, the metalens consists of silicon with a high refractive index, QDs are embedded in SiO₂, and the gold mirror surface at the bottom reflects the single photons radiated downward from the quantum dots into the metalens, thus improving the collection efficiency of the single-photon source radiation. Although the radiation from the QD single-photon source is random, it can always be decomposed into two opposite spin states with left-hand circular polarization and right-hand circular polarization. In order to separate these two spin state emissions along different directions, a geometric phase-based phase mutation can be used to design a metalens. Based on this design, the structure of the silicon-based metalens with bifocal point is obtained by using fluorescence imaging, precise positioning technique, and nano-processing techniques. The optical test results show that for the structure with $\theta_1 = -\theta_2 = 0^\circ$, the half-height widths of the single-photon radiation in the horizontal and vertical directions are 5.47° and 5.99° , respectively, which are basically consistent with the simulated result of 5.8° ; for the structure with $\theta_1 = -\theta_2 = 20^\circ$, the half-height widths of the single-photon radiation in the horizontal and vertical directions are 4.84° and 3.17° , respectively. The polarization of left and right spin polarization is 88% and 78%, respectively. In the following year, the team proposed to place a single QD inside a micro-ring resonant cavity waveguide with second-order angular gratings embedded in the inner wall to enable efficient coupling of the QD with a micro-cavity mode with orbital angular momentum, as shown in Figure 8b [78]. When the two modes are modulated by the angular grating, the mode inside the micro-ring is scattered into free space in a spiral propagation, thus enabling the generation of orbital angular momentum photons. For a micro-ring resonant cavity with a fixed grating number q , where the angular quantum number p of the echo wall mode determines the topological charge number l of the outgoing orbital angular momentum, i.e., $l = \text{sign}(p)(|p| - q)$ [79]. Therefore, the orbital angular momentum mode of the QD producing upward radiation in this micro-ring resonant cavity is a superposition state of order l . To maximize the coupling of the single photons emitted from the QD into the cavity mode, experimentally, they tuned the QD exciton lines to the center of the cavity mode by temperature tuning so that the peak position of the single photons resonates with the peak position of the cavity mode, thus achieving a spontaneous radiation rate enhancement of the quantum dot by the micro-ring resonant cavity by a factor of about 2. The single-photon purity of the single-photon source carrying orbital angular momentum emitted by characterizing the second-order correlation function with zero delays is close to 90%. The near-field and far-field mode distributions obtained from the single-photon emitted light after cavity mode modulation show that the outgoing photons carry a superposition of the orbital angular momentum states.

Inspired by topological phases and phase transitions in condensed matter, a new research field based on topological band theory, topological photonics, has emerged [80,81]. Topological quantum light sources are promoted by the discovery of the topological edge states and corner states with robustness against defects and perturbations. Important results have been achieved in the combination of topological photonics and quantum optics [82], including topologically protected photon pair sources based on the one-dimensional Su–Schrieffer–Heeger (SSH) model and the two-dimensional integer quantum Hall effect [83,84], topologically protected tunable quantum interference [85], etc. On this basis, Dai T. et al. prepared a quantum entangled light source with topology-protected properties by designing multiple micro-ring cavities coupled to each other to form an optically anomalous Floquet topological insulator based on a silicon-based optical quantum chip in a complementary metal-oxide-semiconductor (CMOS) process [86]. However, these topological quantum light sources are not realized based on semiconductor quantum dots. In 2023, Jurkat J. et al. demonstrated a single-photon source based on a single semiconductor QD coupled to a topologically nontrivial SSH cavity mode and provided an in-depth

study of Purcell enhancement ($F_p = 1.8 \pm 0.4$) for this topological quantum light source and demonstrate its emission of nonclassical light (the second-order correlation function of the in resonant QD gives a $g^{(2)}(0) = (0.365 \pm 0.006)$) on demand [87]. Figure 8c shows a sketch of the structure, where the cut through the structures highlights the difference in the cavity layer thickness and, therefore, a difference in the optical confinement potential.

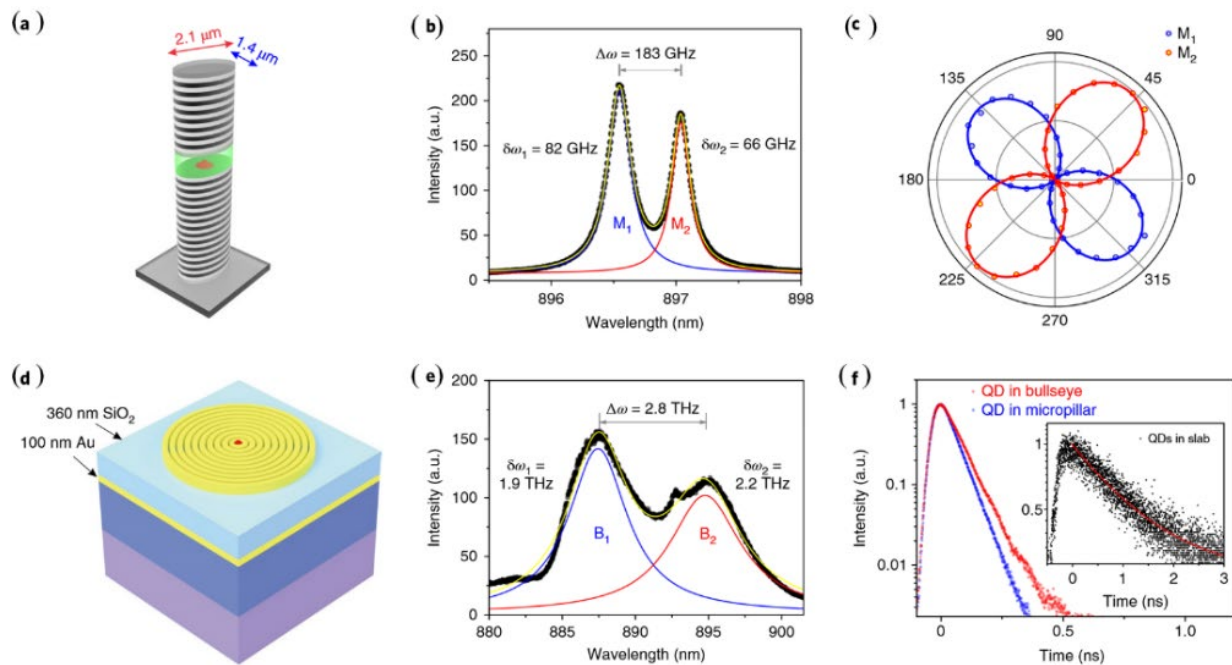


Figure 7. (a) Illustration of the InGaAs QD elliptical micropillar single-photon sources [74]; (b) Two fundamental modes of the elliptical micropillar, M_1 and M_2 ; (c) Polarization-resolved measurement of the two cavity modes, which are perpendicular to one another; (d) Schematic structure of the elliptical CBG, which consists of a central elliptical disk; (e) Two non-degenerate modes of broadband CBG cavity, B_1 and B_2 . The investigated quantum dot is resonant with B_2 ; (f) Radiative lifetime of the quantum dots coupled to the elliptical CBG cavity (red) and in the elliptical micropillar cavity (blue). ((a–f) from Ref [74], reprint with the permission of Springer Nature Publishing).

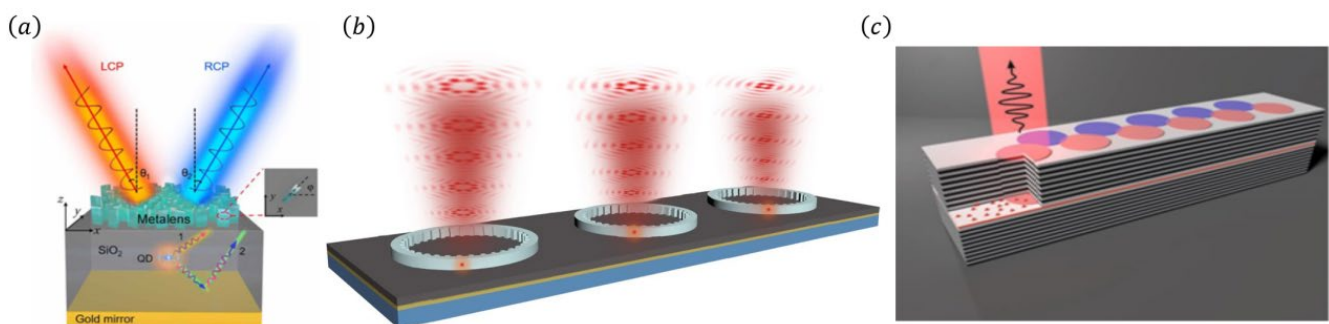


Figure 8. (a) Illustration of the designed structure for manipulating QD emission [77]. The structure consists of three layers: a top metasurface layer, a middle dielectric layer with a QD embedded, and a bottom gold reflector layer; ((a) from Ref [77], licensed under a Creative Commons Attribution (CC BY) license). (b) Schematic of the devices emitting single photons carrying OAM [78]. Single epitaxial QDs are located in each microring with an angular grating patterned along the inner wall; ((b) from Ref [78], reprint with the permission of Springer Nature Publishing). (c) Sketch of an etch-and-overgrowth zigzag chain with $n = 11$ coupled traps [87]. The defect mode is indicated at the left side of the chain; the detuning of the QD to the cavity plotted vs. the intensity of the QD emission shows a clear enhancement at zero detuning. ((c) from Ref [87], reprint with the permission of ACS Publishing).

5. Artificial Microstructures Enhanced Entangled Photon Emission from Semiconductor Quantum Dots

Entangled photon sources are indispensable in the quantum information science and technology field [88,89]. The main methods to generate entangled photon sources are spontaneous parametric down-conversion (SPDC) and spontaneous four-wave mixing (SFWM) of nonlinear crystals. However, these methods not only have low collection efficiency but are also probabilistic in nature, limiting the scalability and reproducibility of entangled photon sources. In contrast, semiconductor quantum dot-based quantum sources can be triggered by external electrical or optical pulses as needed to generate deterministic entangled photon pairs, while the random radiation of photons leads to a low collection efficiency [90]. Artificial microstructures offer the possibility to realize quantum entangled photon sources with high brightness, high entanglement fidelity, and high indistinguishability. Compared to the process of quantum dot generation of single photons, quantum dot generation of entangled photon pairs will have two additional challenges. Firstly, the fine structure cleavage of the quantum dot needs to be smaller than the linewidth of the quantum dot radiating photons so as to post-erase the information of which path the quantum dot double exciton leap comes from. Second, because of the difference in energy between the double exciton $|XX\rangle$ and single exciton $|X\rangle$ jumps, the wavelengths of the two exciton jumps are not equal, which requires the optical resonant cavity to be relatively broadband. Nanowires are a non-cavity waveguide structure, and quantum dots in nanowires can be well coupled into waveguide modes to achieve an efficient collection of entangled photon pairs. The collection bandwidth usually has tens of nanometers, which is suitable for improving the collection efficiency of entangled photon pairs. In 2017, Jöns K. D. et al. used self-organized grown nanowires collected ~ 200 kHz entangled photon pairs at the first lens under 80 MHz pulsed excitation, which was a 20 times enhancement as compared to a bare quantum dot without a photonic nanostructure, and the entanglement fidelity was $81.7\% \pm 0.2\%$ [91]. In 2022, Aumann P et al. have shown the coherent coupling of the ground to biexciton state of an InAsP QD embedded in an InP nanowire via an optimized two-photon resonant excitation scheme and generated time-bin entangled photons, yielding a fidelity of 90% with respect to the maximally entangled Bell state [92]. Microlenses are another commonly used structure for extracting entangled photon pairs. In 2018, Chen Y. et al. built a broadband microlens with an extraction efficiency of $65\% \pm 4\%$ and demonstrated a highly efficient entangled-photon source by collecting strongly entangled photons (fidelity of 90%) at a pair efficiency of $37.2\% \pm 0.2\%$ per pulse [93]. Recently, the team achieved a 1 GHz-clocked, maximally entangled, and on-demand photon-pair source based on droplet etched GaAs QD using two-photon excitation [94]. By using these GaP microlens enhanced entangled photon pair sources in conjunction with their substantial brightness, raw entanglement fidelities of up to $95\% \pm 1\%$, and postselected photon indistinguishability of up to $93\% \pm 1\%$, the suitability for quantum repeater-based long-range quantum entanglement distribution schemes is demonstrated.

In 2019, Liu J. et al. proposed a new CBG cavity on highly efficient broadband reflectors with GaAs QDs based on quantum light radiation control theory, which can overcome the lateral and backward leakage of photons and greatly enhance the Purcell-enhanced emission with high brightness and indistinguishability of entangled photon pairs, as shown in Figure 9a [95]. Using a wide-field QD positioning technique, they deterministically fabricate the new broadband photonic nanostructures in which single GaAs QDs are precisely located at the optimal position (the center of the CBG cavity) for high-performance generation of entangled photon pairs. The solid-state entangled photon source produces entangled photon pairs with a pair collection probability of up to $65\% \pm 4\%$ (single-photon extraction efficiency of $85\% \pm 3\%$ for both $|X\rangle$ and $|XX\rangle$), a high degree of single-photon purity of $99.8\% \pm 0.1\%$, entanglement fidelity of $88\% \pm 2\%$, and indistinguishabilities of $90.1\% \pm 0.3\%$ and $90.3\% \pm 0.3\%$ are simultaneously obtained. In the same year, Wang H. et al. used a CBG-like structure (with a broadband high Purcell

factor of up to 11.3) coupled with InAs QD to achieve generate entangled photon pairs with a state fidelity of $90\% \pm 1\%$, the pair generation rate of $59\% \pm 1\%$, the pair extraction efficiency of $62\% \pm 6\%$, and photon indistinguishability of $90\% \pm 1\%$ simultaneously [96]. In 2022, Rota M. B. et al. demonstrated for the first time the combination of a cavity-enhanced QD entangled photons source and a strain-tuning device capable of tuning the emission energy and the fine structure splitting of the excitonic lines by embedding a single GaAs QD into a CBG cavity and integrated onto a micromachined multiaxial piezoelectric actuator allowing for strain tuning, as shown in Figure 9b [97]. They achieved the extraction efficiency of the emitted entangled photons to a factor of $77\% \pm 5\%$, reaching single photons measured count rates up to $4.1 \times 10^6 \text{ s}^{-1}$ and measured lifetimes down to $(14 \pm 1) \text{ ps}$ for the $|XX\rangle$ transition and $(23 \pm 1) \text{ ps}$ for the $|X\rangle$ transition, corresponding to Purcell factors up to 11. In the same year, Ginés L et al. utilized a micropillar cavity (the QD is deterministically positioned in the center of the micropillar, the top 5 and bottom 18 pairs of $\lambda/4$ AlAs/GaAs DBR forming a cavity) with a low Q factor (280) and demonstrated that such the device with 69.4 (10)% efficiency that features broadband operation suitable for extraction of photon pairs, and the design of the device could be further optimized to allow for extraction efficiency of 85% [98]. The QD is excited collinearly with the axis of the micropillar. The inset represents the two-photon resonant excitation scheme: a laser coherently couples the ground $|g\rangle$ to the biexciton state $|XX\rangle$ through two-photon resonant excitation, the QD system decays to the ground state via exciton state $|X\rangle$, emitting the biexciton-exciton cascade, as shown in Figure 9c.

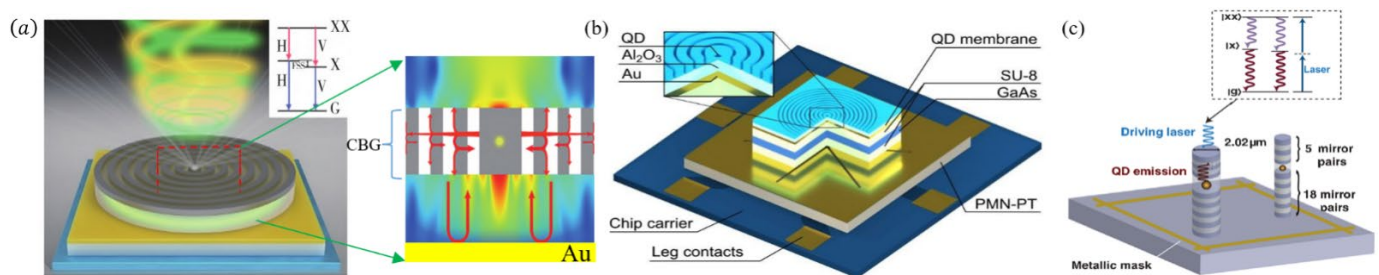


Figure 9. (a) An illustration of a CBG cavity on a highly efficient broadband reflector with a single QD emitting entangled photon pairs. (b) Sketch of the CBG cavity on a six-legged piezoelectric substrate mounted on a chip carrier [97]; ((b) from Ref [97], licensed under a Creative Commons Attribution (CC BY) license). (c) Schematic of the micropillar cavity entangled photon generation and the excitation method [98]. ((c) from Ref [98], licensed under a Creative Commons Attribution 4.0 International License (CC BY 4.0)).

Furthermore, entangled photon generation based on semiconductor QD in the telecom band is of critical importance as it enables the realization of quantum communication protocols over long distances using deployed telecommunication infrastructure [99,100]. However, there are few reports on high-performance semiconductor QD entangled photon sources based on artificial microstructures, which will be one of the key research goals in the future.

6. Conclusions

In summary, the rapid development of quantum information science and technology in recent years requires the demonstration of practical, high-performance single-photon sources and entangled light sources. Self-assembled quantum dots grown based on modern epitaxy techniques [101,102] have an atom-like energy level structure. When combined with pulsed resonance excitation technology, they can generate single-photon quantum emissions that are considered to be of the highest quality nowadays. So, how to achieve deterministic and high quality in semiconductor quantum dot systems, single-photon sources, and entangled photon sources are very important research topics. At present, researchers have used artificial microstructures such as microcavities and metasurfaces and

combined them with the developed topological photonic technology to study the efficient on-demand controllable quantum light source, and the regulation of quantum states such as orbital angular momentum quantum state, spin quantum state, etc., so that the quantum dot quantum light source based on pulse resonance excitation technology in controllability, purity, brightness, full homogeneity, and coherence has been greatly improved and is close to the application level. On the one hand, if the pulsed resonant excitation of quantum dots in the strongly coupled region can be realized, it will greatly improve the generation efficiency and quality of quantum dot quantum light sources; on the other hand, as most of the current research has only realized the out-of-plane radiation of quantum light sources, how to further couple quantum light sources into the chip efficiently and explore the micro and nano-based on quantum information technology, is still a huge challenge, which is also an important research direction for future quantum information research.

In the beginning, single-photon sources based on semiconductor QDs were thought to be not ideal due to their uncontrollability of QD positioning, low device yield, cryogenic working conditions, as well as difficulties in achieving electric pumping. However, after the recent tremendous development, as discussed above, semiconductor QDs are moving toward promising quantum light sources suitable for various applications in the field of quantum information. We have reasons to believe that single-photon sources based on semiconductor QDs are becoming one of the most attractive candidates for the next generation of ideal quantum light sources.

Author Contributions: Writing—original draft preparation, R.L.; writing—review and editing, Q.L.; funding acquisition, F.L. and Q.L. All authors have read and agreed to the published version of the manuscript.

Funding: This research was funded by the National Natural Science Foundation of China (62274014, 62235016); Beijing Municipal Science & Technology Commission (Z221100002722018).

Institutional Review Board Statement: Not applicable.

Informed Consent Statement: Not applicable.

Data Availability Statement: Not applicable.

Conflicts of Interest: The authors declare no conflict of interest.

References

1. Yablonovitch, E. Inhibited Spontaneous Emission in Solid-State Physics and Electronics. *Phys. Rev. Lett.* **1987**, *58*, 2059–2062. [[CrossRef](#)] [[PubMed](#)]
2. Feynman, R.P. Simulating physics with computers. In *Feynman and Computation*; CRC Press: Boca Raton, FL, USA, 2018; pp. 133–153.
3. Xu, F.; Ma, X.; Zhang, Q.; Lo, H.-K.; Pan, J.-W. Secure quantum key distribution with realistic devices. *Rev. Mod. Phys.* **2020**, *92*, 025002. [[CrossRef](#)]
4. Deutsch, D.; Jozsa, R. Rapid solution of problems by quantum computation. *Proc. R. Soc. London. Ser. A Math. Phys. Sci.* **1992**, *439*, 553–558.
5. Bennett, C.H.; Brassard, G.; Crépeau, C.; Jozsa, R.; Peres, A.; Wootters, W.K. Teleporting an unknown quantum state via dual classical and Einstein-Podolsky-Rosen channels. *Phys. Rev. Lett.* **1993**, *70*, 1895. [[CrossRef](#)] [[PubMed](#)]
6. Shor, P.W. Polynomial-time algorithms for prime factorization and discrete logarithms on a quantum computer. *SIAM Rev.* **1999**, *41*, 303–332. [[CrossRef](#)]
7. Grover, L.K. Quantum computers can search arbitrarily large databases by a single query. *Phys. Rev. Lett.* **1997**, *79*, 4709. [[CrossRef](#)]
8. Duan, L.M.; Lukin, M.D.; Cirac, J.I.; Zoller, P. Long-distance quantum communication with atomic ensembles and linear optics. *Nature* **2001**, *414*, 413–418. [[CrossRef](#)]
9. DiVincenzo, D.P. Quantum computation. *Science* **1995**, *270*, 255–261. [[CrossRef](#)]
10. Bao, X.-H.; Reingruber, A.; Dietrich, P.; Rui, J.; Dück, A.; Strassel, T.; Li, L.; Liu, N.-L.; Zhao, B.; Pan, J.-W. Efficient and long-lived quantum memory with cold atoms inside a ring cavity. *Nat. Phys.* **2012**, *8*, 517–521. [[CrossRef](#)]
11. Maccone, L.; Ren, C. Quantum radar. *Phys. Rev. Lett.* **2020**, *124*, 200503. [[CrossRef](#)]
12. O’Brien, J.L.; Furusawa, A.; Vučković, J. Photonic quantum technologies. *Nat. Photonics* **2009**, *3*, 687–695. [[CrossRef](#)]
13. Bloch, I. Quantum coherence and entanglement with ultracold atoms in optical lattices. *Nature* **2008**, *453*, 1016–1022. [[CrossRef](#)]
14. Häffner, H.; Roos, C.F.; Blatt, R. Quantum computing with trapped ions. *Phys. Rep.* **2008**, *469*, 155–203. [[CrossRef](#)]

15. Clarke, J.; Wilhelm, F.K. Superconducting quantum bits. *Nature* **2008**, *453*, 1031–1042. [[CrossRef](#)] [[PubMed](#)]
16. Scappucci, G.; Kloeffer, C.; Zwanenburg, F.A.; Loss, D.; Myronov, M.; Zhang, J.-J.; De Franceschi, S.; Katsaros, G.; Veldhorst, M. The germanium quantum information route. *Nat. Rev. Mater.* **2021**, *6*, 926–943. [[CrossRef](#)]
17. Zhou, L.; Lin, J.; Jing, Y.; Yuan, Z. Twin-field quantum key distribution without optical frequency dissemination. *Nat. Commun.* **2023**, *14*, 928. [[CrossRef](#)]
18. Politi, A.; Cryan, M.J.; Rarity, J.G.; Yu, S.; O'Brien, J.L. Silica-on-silicon waveguide quantum circuits. *Science* **2008**, *320*, 646–649. [[CrossRef](#)]
19. Darquié, B.; Jones, M.P.A.; Dingjan, J.; Beugnon, J.; Bergamini, S.; Sortais, Y.; Messin, G.; Browaeys, A.; Grangier, P. Controlled single-photon emission from a single trapped two-level atom. *Science* **2005**, *309*, 454–456. [[CrossRef](#)]
20. Lounis, B.; Moerner, W.E. Single photons on demand from a single molecule at room temperature. *Nature* **2000**, *407*, 491–493. [[CrossRef](#)]
21. Sipahigil, A.; Jahnke, K.D.; Rogers, L.J.; Teraji, T.; Isoya, J.; Zibrov, A.S.; Jelezko, F.; Lukin, M.D. Indistinguishable photons from separated silicon-vacancy centers in diamond. *Phys. Rev. Lett.* **2014**, *113*, 113602. [[CrossRef](#)]
22. He, Y.M.; Clark, G.; Schaibley, J.R.; Chen, M.-C.; Wei, Y.-J.; Ding, X.; Zhang, Q.; Yao, W.; Xu, X.; Lu, C.-Y.; et al. Single quantum emitters in monolayer semiconductors. *Nat. Nanotechnol.* **2015**, *10*, 497–502. [[CrossRef](#)] [[PubMed](#)]
23. Tran, T.T.; Bray, K.; Ford, M.J.; Toth, M.; Aharonovich, I. Quantum emission from hexagonal boron nitride monolayers. *Nat. Nanotechnol.* **2016**, *11*, 37–41. [[CrossRef](#)] [[PubMed](#)]
24. Senellart, P.; Solomon, G.; White, A. High-performance semiconductor quantum-dot single-photon sources. *Nat. Nanotechnol.* **2017**, *12*, 1026–1039. [[CrossRef](#)] [[PubMed](#)]
25. Michler, P. Nonclassical light from single semiconductor quantum dots. In *Single Quantum Dots: Fundamentals, Applications, and New Concepts*; Springer: Berlin/Heidelberg, Germany, 2003; pp. 315–347.
26. Fischer, K.A.; Müller, K.; Lagoudakis, K.G.; Vučković, J. Dynamical modeling of pulsed two-photon interference. *New J. Phys.* **2016**, *18*, 113053. [[CrossRef](#)]
27. Hanbury Brown, R.; Twiss, R.Q. A test of a new type of stellar interferometer on Sirius. *Nature* **1956**, *178*, 1046–1048. [[CrossRef](#)]
28. Hong, C.K.; Ou, Z.Y.; Mandel, L. Measurement of subpicosecond time intervals between two photons by interference. *Phys. Rev. Lett.* **1987**, *59*, 2044. [[CrossRef](#)]
29. Khitrova, G.; Gibbs, H.M.; Kira, M.; Koch, S.W.; Scherer, A. Vacuum Rabi splitting in semiconductors. *Nat. Phys.* **2006**, *2*, 81–90. [[CrossRef](#)]
30. Vahala, K.J. Optical microcavities. *Nature* **2003**, *424*, 839–846. [[CrossRef](#)]
31. Hennessy, K.; Badolato, A.; Winger, M.; Gerace, D.; Atatüre, M.; Gulde, S.; Fält, S.; Hu, E.L.; Imamoglu, A. Quantum nature of a strongly coupled single quantum dot–cavity system. *Nature* **2007**, *445*, 896–899. [[CrossRef](#)]
32. Reithmaier, J.P.; Sek, G.; Löffler, A.; Hofmann, C.; Kuhn, S.; Reitzenstein, S.; Keldysh, L.V.; Kulakovskii, V.D.; Reinecke, T.L.; Forchel, A. Strong coupling in a single quantum dot–semiconductor microcavity system. *Nature* **2004**, *432*, 197–200. [[CrossRef](#)]
33. Yoshie, T.; Scherer, A.; Hendrickson, J.; Khitrova, G.; Gibbs, H.M.; Rupper, G.; Ell, C.; Shchekin, O.B.; Deppe, D.G. Vacuum Rabi splitting with a single quantum dot in a photonic crystal nanocavity. *Nature* **2004**, *432*, 200–203. [[CrossRef](#)] [[PubMed](#)]
34. Benson, O. Assembly of hybrid photonic architectures from nanophotonic constituents. *Nature* **2011**, *480*, 193–199. [[CrossRef](#)]
35. Kimble, H.J. The quantum internet. *Nature* **2008**, *453*, 1023–1030. [[CrossRef](#)] [[PubMed](#)]
36. Stranski, I.N.; Krastanow, L. Zur Theorie der orientierten Ausscheidung von Ionenkristallen aufeinander. *Mon. Chem. Verwandte Teile And. Wiss.* **1937**, *71*, 351–364. [[CrossRef](#)]
37. Marquez, J.; Geelhaar, L.; Jacobi, K. Atomically resolved structure of InAs quantum dots. *Appl. Phys. Lett.* **2001**, *78*, 2309–2311. [[CrossRef](#)]
38. Gschrey, M.; Gericke, F.; Schüßler, A.; Schmidt, R.; Schulze, J.-H.; Heindel, T.; Rodt, S.; Strittmatter, A.; Reitzenstein, S. In situ electron-beam lithography of deterministic single-quantum-dot mesa-structures using low-temperature cathodoluminescence spectroscopy. *Appl. Phys. Lett.* **2013**, *102*, 251113. [[CrossRef](#)]
39. Nowak, A.K.; Portalupi, S.L.; Giesz, V.; Gazzano, O.; Savio, C.D.; Braun, P.-F.; Karrai, K.; Arnold, C.; Lanco, L.; Sagnes, I.; et al. Deterministic and electrically tunable bright single-photon source. *Nat. Commun.* **2014**, *5*, 3240. [[CrossRef](#)]
40. Lodahl, P.; Mahmoodian, S.; Stobbe, S. Interfacing single photons and single quantum dots with photonic nanostructures. *Rev. Mod. Phys.* **2015**, *87*, 347–400. [[CrossRef](#)]
41. Kim, J.; Benson, O.; Kan, H.; Yamamoto, Y. A single-photon turnstile device. *Nature* **1999**, *397*, 500–503. [[CrossRef](#)]
42. Michler, P.; Kiraz, A.; Becher, C.; Schoenfeld, W.V.; Petroff, P.M.; Zhang, L.; Hu, E.; Imamoglu, A. A quantum dot single-photon turnstile device. *Science* **2000**, *290*, 2282–2285. [[CrossRef](#)]
43. Yuan, Z.; Kardynal, B.E.; Stevenson, R.M.; Shields, A.J.; Lobo, C.J.; Cooper, K.; Beattie, N.S.; Ritchie, D.A.; Pepper, M. Electrically driven single-photon source. *Science* **2002**, *295*, 102–105. [[CrossRef](#)] [[PubMed](#)]
44. Santori, C.; Fattal, D.; Vučković, J.; Solomon, G.S.; Yamamoto, Y. Indistinguishable photons from a single-photon device. *Nature* **2002**, *419*, 594–597. [[CrossRef](#)] [[PubMed](#)]
45. Badolato, A.; Hennessy, K.; Atatüre, M.; Dreiser, J.; Hu, E.; Petroff, P.M.; Imamoglu, A. Deterministic coupling of single quantum dots to single nanocavity modes. *Science* **2005**, *308*, 1158–1161. [[CrossRef](#)] [[PubMed](#)]
46. Chang, W.H.; Chen, W.Y.; Chang, H.S.; Hsieh, T.P.; Chyi, J.I.; Hsu, T.M. Efficient single-photon sources based on low-density quantum dots in photonic-crystal nanocavities. *Phys. Rev. Lett.* **2006**, *96*, 117401. [[CrossRef](#)] [[PubMed](#)]

47. Strauf, S.; Stoltz, N.G.; Rakher, M.T.; Coldren, L.A.; Petroff, P.M.; Bouwmeester, D. High-frequency single-photon source with polarization control. *Nat. Photonics* **2007**, *1*, 704–708. [\[CrossRef\]](#)
48. Press, D.; Göttinger, S.; Reitzenstein, S.; Hofmann, C.; Löffler, A.; Kamp, M.; Forchel, A.; Yamamoto, Y. Photon antibunching from a single quantum-dot-microcavity system in the strong coupling regime. *Phys. Rev. Lett.* **2007**, *98*, 117402. [\[CrossRef\]](#)
49. Toishi, M.; Englund, D.; Faraon, A.; Vucković, J. High-brightness single photon source from a quantum dot in a directional-emission nanocavity. *Opt. Express* **2009**, *17*, 14618–14626. [\[CrossRef\]](#)
50. Claudon, J.; Bleuse, J.; Malik, N.S.; Bazin, M.; Jaffrennou, P.; Gregersen, N.; Sauvan, C.; Lalanne, P.; Gérard, J.-M. A highly efficient single-photon source based on a quantum dot in a photonic nanowire. *Nat. Photonics* **2010**, *4*, 174–177. [\[CrossRef\]](#)
51. Rivoire, K.; Buckley, S.; Majumdar, A.; Kim, H.; Petroff, P.; Vučković, J. Fast quantum dot single photon source triggered at telecommunications wavelength. *Appl. Phys. Lett.* **2011**, *98*, 083105. [\[CrossRef\]](#)
52. Reimer, M.E.; Bulgarini, G.; Akopian, N.; Hocevar, M.; Bavinck, M.B.; Verheijen, M.A.; Bakkers, E.P.; Kouwenhoven, L.P.; Zwiller, V. Bright single-photon sources in bottom-up tailored nanowires. *Nat. Commun.* **2012**, *3*, 737. [\[CrossRef\]](#)
53. Birowosuto, M.D.; Sumikura, H.; Matsuo, S.; Taniyama, H.; van Veldhoven, P.J.; Nötzel, R.; Notomi, M. Fast Purcell-enhanced single photon source in 1550-nm telecom band from a resonant quantum dot-cavity coupling. *Sci. Rep.* **2012**, *2*, 321. [\[CrossRef\]](#) [\[PubMed\]](#)
54. Laucht, A.; Pütz, S.; Günthner, T.; Hauke, N.; Saive, R.; Frédéric, S.; Bichler, M.; Amann, M.-C.; Holleitner, A.W.; Kaniber, M.; et al. A waveguide-coupled on-chip single-photon source. *Phys. Rev. X* **2012**, *2*, 011014. [\[CrossRef\]](#)
55. Munsch, M.; Malik, N.S.; Dupuy, E.; Delga, A.; Bleuse, J.; Gerard, J.-M.; Claudon, J.; Gregersen, N.; Moerk, J. Dielectric GaAs antenna ensuring an efficient broadband coupling between an InAs quantum dot and a Gaussian optical beam. *Phys. Rev. Lett.* **2013**, *110*, 177402. [\[CrossRef\]](#) [\[PubMed\]](#)
56. Gazzano, O.; de Vasconcellos, S.M.; Arnold, C.; Nowak, A.; Galopin, E.; Sagnes, I.; Lanco, L.; Lemaître, A.; Senellart, P. Bright solid-state sources of indistinguishable single photons. *Nat. Commun.* **2013**, *4*, 1425. [\[CrossRef\]](#)
57. He, Y.M.; He, Y.; Wei, Y.J.; Wu, D.; Atature, M.; Schneider, C.; Höfling, S.; Kamp, M.; Lu, C.-Y.; Pan, J.-W. On-demand semiconductor single-photon source with near-unity indistinguishability. *Nat. Nanotechnol.* **2013**, *8*, 213–217. [\[CrossRef\]](#)
58. Madsen, K.H.; Ates, S.; Liu, J.; Javadi, A.; Albrecht, S.M.; Yeo, I.; Stobbe, S.; Lodahl, P. Efficient out-coupling of high-purity single photons from a coherent quantum dot in a photonic-crystal cavity. *Phys. Rev. B* **2014**, *90*, 155303. [\[CrossRef\]](#)
59. Giesz, V.; Portalupi, S.L.; Grange, T.; Antón, C.; De Santis, L.; Demory, J.; Somaschi, N.; Sagnes, I.; Lemaître, A.; Lanco, L.; et al. Cavity-enhanced two-photon interference using remote quantum dot sources. *Phys. Rev. B* **2015**, *92*, 161302. [\[CrossRef\]](#)
60. Gschrey, M.; Thoma, A.; Schnauber, P.; Seifried, M.; Schmidt, R.; Wohlfeil, B.; Krüger, L.; Schulze, J.-H.; Heindel, T.; Burger, S.; et al. Highly indistinguishable photons from deterministic quantum-dot microlenses utilizing three-dimensional in situ electron-beam lithography. *Nat. Commun.* **2015**, *6*, 7662. [\[CrossRef\]](#)
61. Sapienza, L.; Davanço, M.; Badolato, A.; Srinivasan, K. Nanoscale optical positioning of single quantum dots for bright and pure single-photon emission. *Nat. Commun.* **2015**, *6*, 7833. [\[CrossRef\]](#)
62. Ding, X.; He, Y.; Duan, Z.-C.; Gregersen, N.; Chen, M.-C.; Unsleber, S.; Maier, S.; Schneider, C.; Kamp, M.; Höfling, S.; et al. On-demand single photons with high extraction efficiency and near-unity indistinguishability from a resonantly driven quantum dot in a micropillar. *Phys. Rev. Lett.* **2016**, *116*, 020401. [\[CrossRef\]](#)
63. Somaschi, N.; Giesz, V.; De Santis, L.; Lored, J.C.; Almeida, M.P.; Hornecker, G.; Portalupi, S.L.; Grange, T.; Antón, C.; Demory, J.; et al. Near-optimal single-photon sources in the solid state. *Nat. Photonics* **2016**, *10*, 340–345. [\[CrossRef\]](#)
64. Heindel, T.; Thoma, A.; von Helversen, M.; Schmidt, M.; Schlehn, A.; Gschrey, M.; Schnauber, P.; Schulze, J.-H.; Strittmatter, A.; Beyer, J.; et al. A bright triggered twin-photon source in the solid state. *Nat. Commun.* **2017**, *8*, 14870. [\[CrossRef\]](#) [\[PubMed\]](#)
65. Su, R.; Liu, S.; Wei, Y.; Yu, Y.; Liu, J.; Yu, S.; Wang, X. Bright and pure single-photons from quantum dots in micropillar cavities under up-converted excitation. *Sci. Bull.* **2018**, *63*, 739–742. [\[CrossRef\]](#) [\[PubMed\]](#)
66. Rutckaia, V.; Heyroth, F.; Novikov, A.; Shaleev, M.; Petrov, M.; Schilling, J. Quantum dot emission driven by Mie resonances in silicon nanostructures. *Nano Lett.* **2017**, *17*, 6886–6892. [\[CrossRef\]](#)
67. Kroychuk, M.K.; Shorokhov, A.S.; Yagudin, D.F.; Rakhlin, M.V.; Klimko, G.V.; Toropov, A.A.; Shubina, T.V.; Fedyanin, A.A. Quantum Dot Photoluminescence Enhancement in GaAs Nanopillar Oligomers Driven by Collective Magnetic Modes. *Nanomaterials* **2023**, *13*, 507. [\[CrossRef\]](#)
68. Moczala-Dusanowska, M.; Dusanowski, L.; Iff, O.; Huber, T.; Kuhn, S.; Czystanowski, T.; Schneider, C.; Höfling, S. Strain-tunable single-photon source based on a circular Bragg grating cavity with embedded quantum dots. *ACS Photonics* **2020**, *7*, 3474–3480. [\[CrossRef\]](#)
69. Li, X.; Liu, S.; Wei, Y.; Ma, J.; Song, C.; Yu, Y.; Su, R.; Geng, W.; Ni, H.; Liu, H.; et al. Bright semiconductor single-photon sources pumped by heterogeneously integrated micropillar lasers with electrical injections. *Light Sci. Appl.* **2023**, *12*, 65. [\[CrossRef\]](#)
70. Chen, Z.S.; Ma, B.; Shang, X.J.; Ni, H.Q.; Wang, J.L.; Niu, Z.C. Bright single-photon source at 1.3 μm based on InAs bilayer quantum dot in micropillar. *Nanoscale Res. Lett.* **2017**, *12*, 378. [\[CrossRef\]](#)
71. Liu, F.; Brash, A.J.; O'Hara, J.; Martins, L.M.P.P.; Phillips, C.; Coles, R.J.; Royall, B.; Clarke, E.; Benthams, C.; Prtljaga, N.; et al. High Purcell factor generation of indistinguishable on-chip single photons. *Nat. Nanotechnol.* **2018**, *13*, 835–840. [\[CrossRef\]](#)
72. Kolatschek, S.; Nawrath, C.; Bauer, S.; Huang, J.; Fischer, J.; Sittig, R.; Jetter, M.; Portalupi, S.L.; Michler, P. Bright Purcell enhanced single-photon source in the telecom O-band based on a quantum dot in a circular Bragg grating. *Nano Lett.* **2021**, *21*, 7740–7745. [\[CrossRef\]](#)

73. Xu, S.-W.; Wei, Y.-M.; Su, R.-B.; Li, X.-S.; Huang, P.-N.; Liu, S.-F.; Huang, X.-Y.; Yu, Y.; Liu, J.; Wang, X.-H. Bright single-photon sources in the telecom band by deterministically coupling single quantum dots to a hybrid circular Bragg resonator. *Photonics Res.* **2022**, *10*, B1–B6. [\[CrossRef\]](#)
74. Wang, H.; He, Y.M.; Chung, T.H.; Hu, H.; Yu, Y.; Chen, S.; Ding, X.; Chen, M.-C.; Qin, J.; Yang, X.; et al. Towards optimal single-photon sources from polarized microcavities. *Nat. Photonics* **2019**, *13*, 770–775. [\[CrossRef\]](#)
75. Wang, X.-L.; Cai, X.-D.; Su, Z.-E.; Chen, M.-C.; Wu, D.; Li, L.; Liu, N.-L.; Lu, C.-Y.; Pan, J.-W. Quantum teleportation of multiple degrees of freedom of a single photon. *Nature* **2015**, *518*, 516–519. [\[CrossRef\]](#) [\[PubMed\]](#)
76. Stav, T.; Faerman, A.; Maguid, E.; Oren, D.; Kleiner, V.; Hasman, E.; Segev, M. Quantum entanglement of the spin and orbital angular momentum of photons using metamaterials. *Science* **2018**, *361*, 1101–1104. [\[CrossRef\]](#) [\[PubMed\]](#)
77. Bao, Y.; Lin, Q.; Su, R.; Zhou, Z.-K.; Song, J.; Li, J.; Wang, X.-H. On-demand spin-state manipulation of single-photon emission from quantum dot integrated with metasurface. *Sci. Adv.* **2020**, *6*, eaba8761. [\[CrossRef\]](#)
78. Chen, B.; Wei, Y.; Zhao, T.; Liu, S.; Su, R.; Yao, B.; Yu, Y.; Liu, J.; Wang, X. Bright solid-state sources for single photons with orbital angular momentum. *Nat. Nanotechnol.* **2021**, *16*, 302–307. [\[CrossRef\]](#)
79. Cai, X.; Wang, J.; Strain, M.J.; Johnson-Morris, B.; Zhu, J.; Sorel, M.; O’Brien, J.L.; Thompson, M.G.; Yu, S. Integrated compact optical vortex beam emitters. *Science* **2012**, *338*, 363–366. [\[CrossRef\]](#)
80. Lu, L.; Joannopoulos, J.D.; Soljačić, M. Topological photonics. *Nat. Photonics* **2014**, *8*, 821–829. [\[CrossRef\]](#)
81. Ozawa, T.; Price, H.M.; Amo, A.; Goldman, N.; Hafezi, M.; Lu, L.; Rechtsman, M.C.; Schuster, D.; Simon, J.; Zilberberg, O.; et al. Topological photonics. *Rev. Mod. Phys.* **2019**, *91*, 015006. [\[CrossRef\]](#)
82. Yan, Q.; Hu, X.; Fu, Y.; Lu, C. Quantum topological photonics. *Adv. Opt. Mater.* **2021**, *9*, 2001739. [\[CrossRef\]](#)
83. Blanco-Redondo, A.; Bell, B.; Oren, D.; Eggleton, B.J.; Segev, M. Topological protection of biphoton states. *Science* **2018**, *362*, 568–571. [\[CrossRef\]](#) [\[PubMed\]](#)
84. Mittal, S.; Goldschmidt, E.A.; Hafezi, M. A topological source of quantum light. *Nature* **2018**, *561*, 502–506. [\[CrossRef\]](#) [\[PubMed\]](#)
85. Mittal, S.; Orre, V.V.; Goldschmidt, E.A.; Hafezi, M. Tunable quantum interference using a topological source of indistinguishable photon pairs. *Nat. Photonics* **2021**, *15*, 542–548. [\[CrossRef\]](#)
86. Dai, T.; Ao, Y.; Bao, J.; Mao, J.; Chi, Y.; Fu, Z.; You, Y.; Chen, X.; Zhai, C.; Tang, B.; et al. Topologically protected quantum entanglement emitters. *Nat. Photonics* **2022**, *16*, 248–257. [\[CrossRef\]](#)
87. Jurkat, J.; Klemmt, S.; De Gregorio, M.; Meinecke, M.; Buchinger, Q.; Harder, T.H.; Beierlein, J.; Egorov, O.A.; Emmerling, M.; Krause, C.; et al. Single-Photon Source in a Topological Cavity. *Nano Lett.* **2023**, *23*, 820–826. [\[CrossRef\]](#)
88. Stevenson, R.M.; Young, R.J.; Atkinson, P.; Cooper, K.; Ritchie, D.A.; Shields, A.J. A semiconductor source of triggered entangled photon pairs. *Nature* **2006**, *439*, 179–182. [\[CrossRef\]](#)
89. Schimpf, C.; Reindl, M.; Huber, D.; Lehner, B.; Da Silva, S.F.C.; Manna, S.; Vyvlecka, M.; Walther, P.; Rastelli, A. Quantum cryptography with highly entangled photons from semiconductor quantum dots. *Sci. Adv.* **2021**, *7*, eabe8905. [\[CrossRef\]](#)
90. Orioux, A.; Versteegh, M.A.M.; Jöns, K.D.; Ducci, S. Semiconductor devices for entangled photon pair generation: A review. *Rep. Prog. Phys.* **2017**, *80*, 076001. [\[CrossRef\]](#)
91. Jöns, K.D.; Schweickert, L.; Versteegh, M.A.M.; Dalacu, D.; Poole, P.J.; Gulinatti, A.; Giudice, A.; Zwiller, V.; Reimer, M.E. Bright nanoscale source of deterministic entangled photon pairs violating Bell’s inequality. *Sci. Rep.* **2017**, *7*, 1700. [\[CrossRef\]](#)
92. Aumann, P.; Prilmüller, M.; Kappe, F.; Ostermann, L.; Dalacu, D.; Poole, P.J.; Ritsch, H.; Lechner, W.; Weihs, G. Demonstration and modeling of time-bin entangled photons from a quantum dot in a nanowire. *AIP Adv.* **2022**, *12*, 055115. [\[CrossRef\]](#)
93. Chen, Y.; Zopf, M.; Keil, R.; Ding, F.; Schmidt, O.G. Highly-efficient extraction of entangled photons from quantum dots using a broadband optical antenna. *Nat. Commun.* **2018**, *9*, 2994. [\[CrossRef\]](#) [\[PubMed\]](#)
94. Hopfmann, C.; Nie, W.; Sharma, N.L.; Weigelt, C.; Ding, F.; Schmidt, O.G. Maximally entangled and gigahertz-clocked on-demand photon pair source. *Phys. Rev. B* **2021**, *103*, 075413. [\[CrossRef\]](#)
95. Liu, J.; Su, R.; Wei, Y.; Yao, B.; da Silva, S.F.C.; Yu, Y.; Iles-Smith, J.; Srinivasan, K.; Rastelli, A.; Li, J.; et al. A solid-state source of strongly entangled photon pairs with high brightness and indistinguishability. *Nat. Nanotechnol.* **2019**, *14*, 586–593. [\[CrossRef\]](#) [\[PubMed\]](#)
96. Wang, H.; Hu, H.; Chung, T.H.; Qin, J.; Yang, X.; Li, J.-P.; Liu, R.-Z.; Zhong, H.-S.; He, Y.-M.; Ding, X.; et al. On-demand semiconductor source of entangled photons which simultaneously has high fidelity, efficiency, and indistinguishability. *Phys. Rev. Lett.* **2019**, *122*, 113602. [\[CrossRef\]](#)
97. Rota, M.B.; Krieger, T.M.; Buchinger, Q.; Beccaceci, M.; Neuwirth, J.; Huet, H.; Horová, N.; Lovicu, G.; Ronco, G.; da Silva, S.F.C.; et al. A source of entangled photons based on a cavity-enhanced and strain-tuned GaAs quantum dot. *arXiv* **2022**, arXiv:2212.12506.
98. Ginés, L.; Moczala-Dusanowska, M.; Dłaka, D.; Hošák, R.; Gonzales-Ureta, J.R.; Lee, J.; Ježek, M.; Harbord, E.; Oulton, R.; Höfling, S.; et al. High extraction efficiency source of photon pairs based on a quantum dot embedded in a broadband micropillar cavity. *Phys. Rev. Lett.* **2022**, *129*, 033601. [\[CrossRef\]](#)
99. Zeuner, K.D.; Jons, K.D.; Schweickert, L.; Hedlund, C.R.; Lobato, C.N.; Lettner, T.; Wang, K.; Gyger, S.; Schöll, E.; Steinhauer, S.; et al. On-demand generation of entangled photon pairs in the telecom C-band with InAs quantum dots. *ACS Photonics* **2021**, *8*, 2337–2344. [\[CrossRef\]](#)

100. Lettner, T.; Gyger, S.; Zeuner, K.D.; Schweickert, L.; Steinhauer, S.; Hedlund, C.R.; Stroj, S.; Rastelli, A.; Hammar, M.; Trotta, R.; et al. Strain-controlled quantum dot fine structure for entangled photon generation at 1550 nm. *Nano Lett.* **2021**, *21*, 10501–10506. [[CrossRef](#)]
101. Liu, F.Q.; Li, L.; Wang, L.; Liu, J.; Zhang, W.; Zhang, Q.; Liu, W.; Lu, Q.; Wang, Z. Solid source MBE growth of quantum cascade lasers. *Appl. Phys. A* **2009**, *97*, 527–532. [[CrossRef](#)]
102. Fei, T.; Zhai, S.; Zhang, J.; Lu, Q.; Zhuo, N.; Liu, J.; Wang, L.; Liu, S.; Jia, Z.; Li, K.; et al. 3 W Continuous-Wave Room Temperature Quantum Cascade Laser Grown by Metal-Organic Chemical Vapor Deposition. *Photonics* **2023**, *10*, 47. [[CrossRef](#)]

Disclaimer/Publisher’s Note: The statements, opinions and data contained in all publications are solely those of the individual author(s) and contributor(s) and not of MDPI and/or the editor(s). MDPI and/or the editor(s) disclaim responsibility for any injury to people or property resulting from any ideas, methods, instructions or products referred to in the content.